Flow Control and High-Lift Performance for Flying-Wing Unmanned Combat Air Vehicle Configurations by inserting slots

U Ali[1]*, E Chadwick[2]

1. University of Salford, School of Computing, Science & Engineering, Salford, United Kingdom

2. University of Salford, School of Computing, Science & Engineering, Salford, United Kingdom

ABSTRACT

The objectives of the present study on Unmanned Combat Air Vehicles (UCAVs) are two-fold: first to control the flow by inserting leading-edge and cross-flow slots and analysing the viscous flow development over the outer panels of a flying-wing configuration to maximise the performance of the elevons control surfaces; second to predict high-lift performance particularly the maximum-lift characteristics. This is demonstrated using a variety of inviscid Vortex Lattice Method (VLM) and Euler, and viscous CFD Reynolds Averaged Navier-Stokes (RANS) methods. The computational results are validated against experiment measured in a wind tunnel. Two flying-wing planforms are considered based around a generic 40° edge-aligned configuration. The VLM predicts a linear variation of lift and pitching moment with incidence angle, and substantially under-predicts the induced drag. Results obtained from RANS and Euler agree well with experiment.

1. INTRODUCTION

The current generation of flying-wing UCAVs lack conventional stabilising surfaces or the associated control surfaces, and as a result in its purest form air vehicles suffer from the inherent disadvantage of being unstable and difficult to control [1]. Modern flying-wing UCAV configurations under consideration here are shown in Figure 1. These aerial vehicles are largely similar in design with geometric features chosen for stealth reasons. The leading and trailing edges of flying-wing configurations are significantly different to those employed on current air vehicles and are found to be not optimal from a purely aerodynamic point of view [2]. Due to Radar Cross Section (RCS) signature and weight constraints, leading and trailing edges have to be aligned at a common angle of between 40° and 60°, resulting in aerodynamic design between pure deltas, diamond and lambda wings. These delta shaped flying-wing configurations allow the air vehicle to operate at near and post stall regimes taking advantage of the additional lift generated by the leading edge vortices [1]. Therefore, detailed understanding of the leading edge vortices behaviour becomes mandatory in order to enhance the air vehicle's performance and manoeuvrability.

The highly-swept leading edges of these configurations promote separated-vortex flows at moderate-to-high incidence angles, enhancing lift generation but resulting in substantially-increased induced drag. Leading edge vortex (LEV) is the main feature of the flow over swept

*Corresponding Author: u.ali4@edu.salford.ac.uk

wings which provide lift for flight control at high angles of attack [3]. A disadvantage, however, is that as the angle of attack is increased, the leading edge vortices become detached and experience a forward migration to the outboard section of the wing. The intensity of this forward migration of flow to the outer panels of the vehicle grow significantly in high angles of attack regime [4].

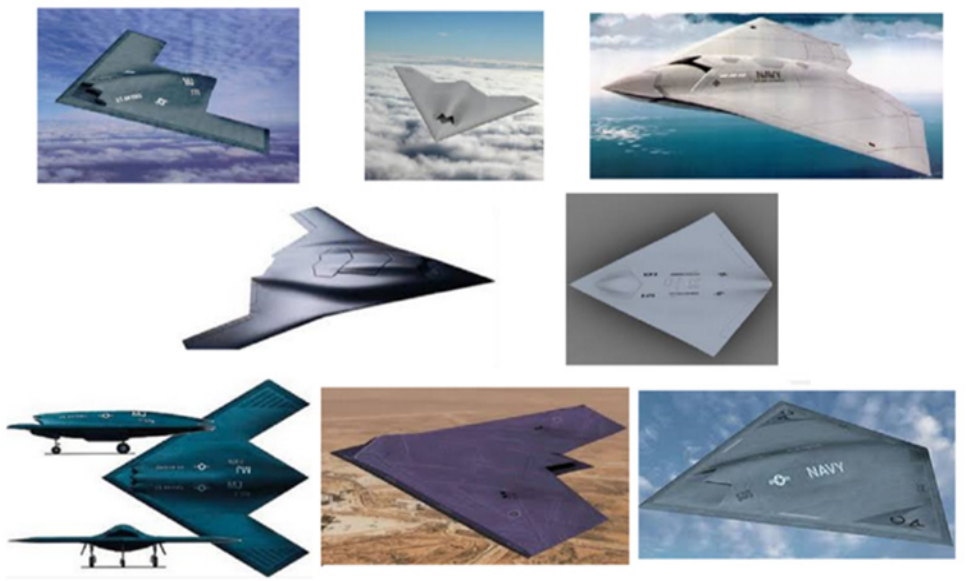

Figure 1: Highly swept flying wing UCAV configurations

As a result of this forward migration to the outer panels of the vehicle, the roll control contributed by the control surfaces becomes severely restricted, since they would be operating in a separated flow [5]. Furthermore, boundary layer flow separation on the outboard wing panels of the configurations is a limiting factor in the ability to exploit the high lift generated by the leading edge vortices.

To address these problems, current research has focused on passive flow-control techniques such as leading-edge flaps, canards and fences [6] [7] [8] [9]. These flow-control techniques, however, cannot be implemented on representative flying-wing configurations due to RCS constraints. Leading edge flaps and vertical fences can have detrimental effects on RCS signature, hence they must be avoided [10].

Instead in this paper leading-edge and cross-flow slots are inserted for the first time on a flying-wing configuration and they successfully control the flow by maximising the flow rate over control surfaces, which in turn enhance the operational control of the vehicle [11]. The slots are flushed with the surface of the wing and as a result the effect on RCS signature is significantly reduced compared to standard flow-control techniques. Leading-edge slots have been used before on straight-wing vehicles but to delay the stall angle to a higher angle of attack [8], not in the context of passive flow control used here. The authors have not found any literature on cross-flow slots, either on flying-wing configurations or flow control, so this appears to be novel strand of research.

2. AERODYNAMICS OF FLYING-WING

2.1. Flow Physics

Although all types of wings are expected to suffer from flow separation at high angles of attack due to viscous effects, sharp edge swept wings are particularly affected by this phenomena. The flying-wing aerial vehicles are used in stealth technology because their flat surfaces and sharp edges help reduce the radar signature of air vehicles [1]. At subsonic speeds, the aerodynamic behaviour of swept wings is different than the high aspect ratio wings. The performance of a flying wing air vehicle, as the one shown in Figure 2, is crucial at low speeds as the mission roles of modern air vehicles require them to operate at low speed and variety of alpha conditions during various flight phases such as take-off and landing [12].

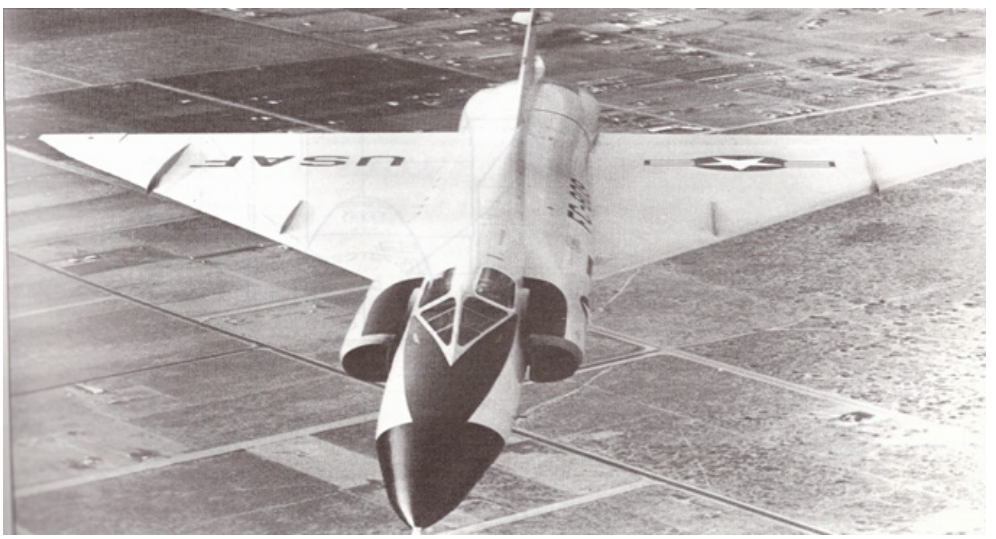

Figure 2: Delta wing air vehicle

Experimental investigations have established that at relatively low angles of attack the flow separates from the leading edges and rolls into two vortex sheets cores, also known as cone-shaped cores, of rotating fluid as illustrated in Figure 3. The vortex type flow is induced due to sharp leading edges of the wing and results in the delay of stall to much higher angles of attack. At moderate angles of attack, the incoming flow impinges on the suction side of the wing and is swept outboard towards the outer panels on the wing.

The separated boundary layer, under the influence of vorticity contained within it, rolls up in a spiral fashion to form a primary vortex pair, shown in Figure 3 [13]. The inner core region in the centre of the vortex is influenced by the viscous forces and has characteristics of large velocity and pressure gradients. The core gives rise to strong swirling velocities and associated with this a strong negative pressure on suction side of the wing [14]. Leading edge vortices are source of high energy and as a result local static pressure in the vicinity of vortices becomes small. Therefore, surface pressure remains constant over the middle of the wing and is reduced considerably near the leading edges as shown in Figure 4. This results in strong suction on the upper surface of the wing as depicted by the vertical arrows in Figure 4. This suction effect is the cause of lift enhancement over delta wings, and this is why delta wing

configurations obtain much higher lift of coefficient for angles of attack at which conventional wings would have stalled [12]. The additional lift achieved by delta wing by delta wing due to leading edge vortices is typically known as non-linear or vortex-lift [15]. The velocity of the fluid within the primary vortex causes significant pressure drop on upper surface of the wing and as a result high lift is achieved due to pressure difference between upper and lower surface of the wing [13].

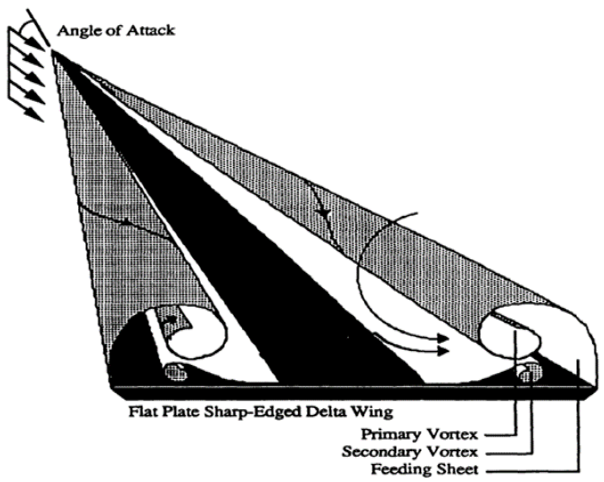

Figure 3: Schematic view of leading edge formation on a flat plate delta wing

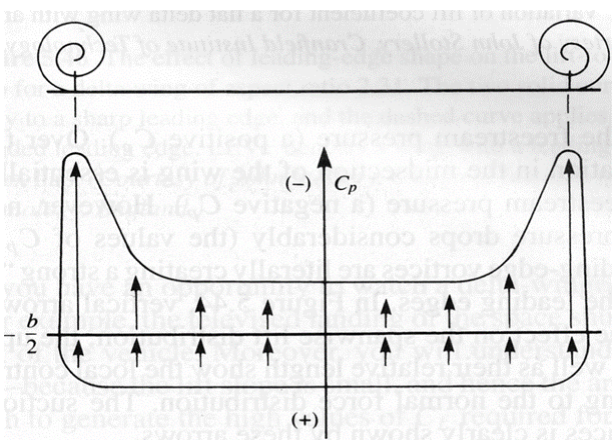

Figure 4: Schematic of the spanwise pressure coefficient distribution across a delta wing

The aerodynamic characteristics of flying-wing configurations are considered to be a strong function of the angle of attack and sweep angle of wing. The thickness and leading edge geometry of the wing can also affect the flow physics of swept wings but dependence on Reynolds number is not as strong for delta wings with sharp edges. Therefore, aerodynamic forces such as lift and moments do not change substantially with Reynolds number, compared to stronger factors such as incidence and wing sweep [16].

2.2. Radar Cross Section

Radio detection and ranging or more commonly known as Radar, transmit radio waves to detect the presence of an aircraft and find its position. The principle of radar is that a transmitter sends out radio signals which are reflected back to the source or a receiver when an object is encountered [17]. When transmitter and receiver are located on same platform and share the antenna, the radar is called monostatic. The radar is referred as bistatic, when radar transmitter and receiver are at two different locations. Although stealth aircraft is not completely invisible to radar, but to remain undetected the aircraft must be designed with the smallest possible radar cross section (RCS), so that its return is below the detection threshold of the radar [18].

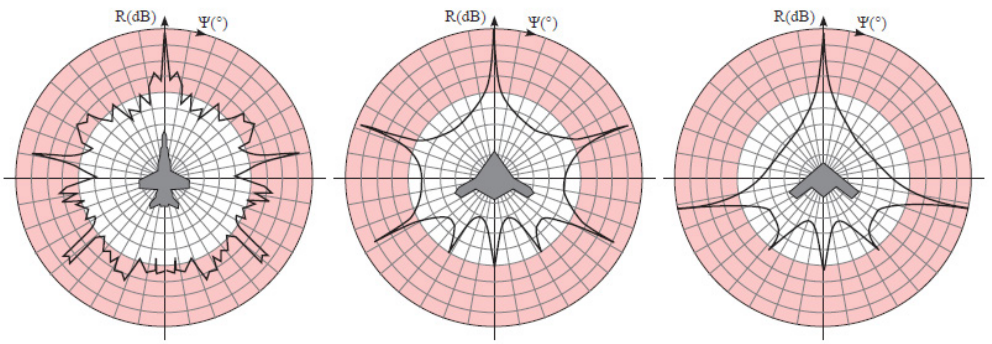

Figure 5: Radar Cross Section signature at 9GHz (a) F-18E Super Hornet, (b) Northrup Grumman X-47B and (c) Generic 40° Swept UCAV [19]

RCS is a measure of how detectable an aircraft is when encountered by the radio signals. Radar cross section of aircraft can be minimised by planform alignment and materials selection for the airframe [10]. The planform alignment is an airframe design strategy in which leading and trailing edges are aligned in a particular direction in order to direct radar energy away from the source into space. The planform alignment or shaping of a stealth aircraft is generally considered to be most important line of RCS control. The shaping of these aerial vehicles leads to unconventional planform shapes that are associated with the term stealth. The stealth designs are aerodynamically unstable because vertical tails and control surfaces are avoided on these aerial vehicles. For the aircraft with curved or perpendicular surfaces, the returns to the source will be strong [10]. An example of this phenomena is shown in Figure 5 where a conventional fighter aircraft is compared with two stealth UCAVs. It can be seen that edge aligned planforms have much lower broadband response and reflections take the form of spikes. The other way of minimising aircraft's RCS signature is by using radar absorbing materials (RAM). Those materials absorb and attenuate radar energy rather than reflect it [18].

2.3. Flow Control

In order to meet RCS demands on flying-wing configurations under consideration here, the vertical tails or the associated control surfaces have to be avoided which makes aerodynamic stability and control a special problem for an air vehicle [1]. The present work explores the flow control mechanisms which can reattach or postpone the flow separation on outer wing

panels, which in turn should lead to lift enhancement, stall delay, and roll control in high angles of attack regime. Flow control can be defined as the ability to manipulate a flow field to effect a desired change. Control of flow is generally classified into active and passive control of the flow structures [20].

Active flow control requires some form of energy input or auxiliary power in order to manipulate the flow structure over the wing. Passive control, on the other hand, do not require any energy input and any feedback mechanism. This method of flow-control has been applied by adding control surfaces to the wing such as canards, flaps, strakes, and leading edge fences. In past, passive lift enhancements for delta wings have been demonstrated as a potential method for the control of vortex dominated swept wing flows. Even to this day, passive flow-control remains the most used mode of flow-control method. Vortex generators, for example, are currently employed on the wings of most Boeing aircrafts in order to control flow separation on the wings [20]. In present study, however, it is not feasible to add such control surfaces due to their adverse effect on radar cross section (RCS) signature. As a result, novel flow control mechanisms need to be investigated in order to manipulate the flow field over swept wings without leading to loss of control. The challenge is to achieve that change with a simple device that is inexpensive to build and operate, and has minimum side effects with respect to RCS signature.

3. RESEARCH METHODOLOGY

The investigation of the flow development over two flying-wing configurations was carried out using a mixture of computational and experimental approaches. In particular, low speed high lift characteristics involving vortex separated flows were investigated experimentally in subsonic wind tunnel facilities. In order to analyse the lift characteristics and flow control on representative flying-wing configurations, it was deemed necessary to carry out experimental and numerical analysis on clean baseline models before implementing a flow control mechanism on flying-wing configurations under investigation. For this purpose, the investigations were carried out on two flying-wing models shown in figure 6.

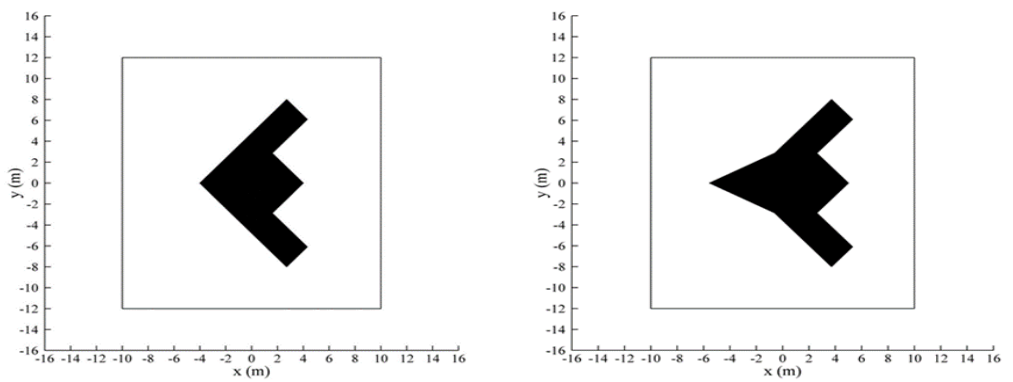

Figure 6: UCAV planform geometries used for experimental and computational investigations: 40° configuration (left); and 40° with 60° cranked configuration (right)

One of those two models has a sweep angle of 40 degrees and a root chord of 0.4m and is called Configuration 1 in this study. The other cranked flying-wing model has a leading edge

sweep angle of 60 degrees and a root chord of 0.53m and is called Configuration 2. An experimental and computational investigations conducted in this study have focused on both low and large angles of attack in order to include the formation of the leading edge vortices, the onset of vortex breakdown, and the onset of fully separated flow. The wind tunnel tests on flying-wing configurations have served two fold purpose of shedding light on relevant flow phenomena and have also provided experimental data for validation and evaluation of computational methods. The computational methods ranging from vortex-lattice methods to Euler and RANS computational fluid dynamics (CFD) were employed in order to evaluate the flow physics on flying-wing configurations and to validate the experimental data.

3.1. Experimental Approach

An experimental investigation was performed in a low speed wind tunnel using two different flat-plate scale models, Configuration 1 and Configuration 2. These wind tunnel models were constructed in the aeronautical laboratory using aluminium. The models have a thickness of 3mm, and their leading and side edges were chamfered in order to help formation of leading-edge vortices. Wind tunnel tests were repeated in order to ensure consistency within results. The wind tunnel used for the investigation is a low speed closed return tunnel with a test section size of 0.85m × 1.15m. The test facility has a maximum speed of 36 m/s and a turbulence intensity of 0.5%. There is a honeycomb mesh upstream of the settling chamber to reduce transverse turbulence. The test section has a 6-component beam balance with strut mountings, in order to support the models. The model was mounted on a six component force balance as shown in Figure 7. Three components measured the forces in three axes and the remaining three measured the moments about three axes. Initially, incidence angle was zero and the output of six component balance was recorded as static or wind off values. The wind tunnel was then switched on and the free stream velocity was adjusted to approximately 32 m/s and the output of six component balance was recorded as dynamic values.

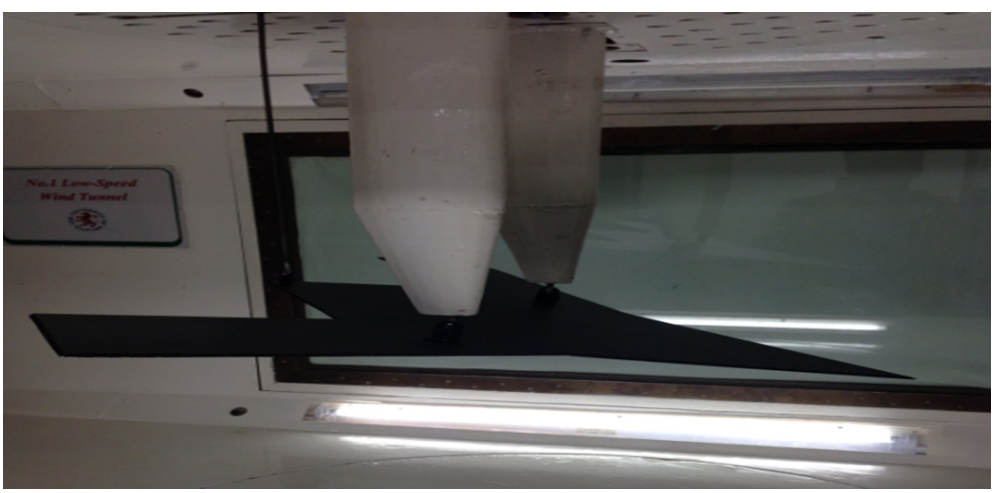

Figure 7: UCAV Configuration 2 mounted in a low speed wind tunnel

The angle of attack was changed by an interval of 2.5° and the dynamic output for each angle of attack was recorded. When flow conditions had stabilised, the data was collected for a

period of 20 seconds and within that time, 100 samples points were recorded by the data acquisition recorder. At each angle of attack the wind off values are subtracted from dynamic values and then multiplied with wind tunnel correction matrix. In order to obtain non-dimensional forces, the data is finally divided by the dynamic pressure and reference area.

3.2. CFD Approach

All the CFD simulations in this study have been carried out in two types of CFD codes: a commercial CFD code Fluent was used to conduct turbulent CFD simulations, and an in-house CFD solver was used to perform non-linear Euler simulations. Fluent solved the compressible, three dimensional Reynolds averaged Navier-Stokes (RANS) equations in a cell centred finite-volume formulation to calculate the solution at hand. The results for clean baseline models were compared with experimental data and Inviscid linear technique called Vortex Lattice Method (VLM). Leading edge cavity and cross flow cavity techniques were studied using RANS, as a passive flow control method and results were compared with wind tunnel tests. Initial efforts were focused on computing and understanding the aerodynamic characteristics of baseline flying-wing configurations, which itself was a challenge due to the complexity of flow field.

3.2.1. Geometry and Grid details

In this study, all the CAD models used for turbulent flow simulations were created in SolidWorks. The detailed dimensions of both configurations are shown in Figures 8 and 9. The flying-wing configurations created in SolidWorks are then exported to a grid generator using Industrial Standard File Formats such as IGES, STEP. In this research both structured and unstructured grids have been used to perform the investigations under discussion. Although it takes much more effort to generate structured grids around three dimensional configurations but they are widely regarded to be superior to unstructured meshes for boundary layer problems. CAE systems grid generator, called ANSA, was used to generate structured meshes in this study. Three dimensional grids for clean baseline configurations used is this study are shown in Figures 10 and 11. Only half span of the models were meshed because symmetric boundary conditions are examined for both clean baseline models and the model in which slots were used as a flow control mechanism. To ensure grid independent results, three different meshes for configuration 1, and four different meshes for configuration 2 were generated where grid size was increased from coarse to medium and then fine and very fine. The simulations for these grids were performed for the cases where angle of attacks generated maximum lift for respective configurations. Table 1 and 2 show the lift and drag coefficients that were obtained from all the simulations and results are compared with experimental data.

Table 1: Comparing grid refinement results for Configuration 1 at incidence angle of 19.197°

	Nodes on UCAV		**Max Y+**	**CL**	**CD**
	Chordwise	**Spanwise**			
Experiment	-	-	-	0.93780	0.35441
0.5m	49	63	0.62	0.90282	0.31589
1.0m	56	73	0.57	0.90957	0.31633
2.0m	65	85	0.89	0.91807	0.31796

Table 2: Comparing grid refinement results for Configuration 2 at incidence angle of 29.041°

	Nodes of UCAV		Max Y+	CL	CD
	Chordwise	Spanwise			
Experiment	-	-	-	1.13243	0.75249
0.5m	52	61	0.66	1.06686	0.61261
1m	69	81	0.58	1.09242	0.62653
2m	76	89	0.62	1.11015	0.63146
3m	83	98	0.38	1.12047	0.63725

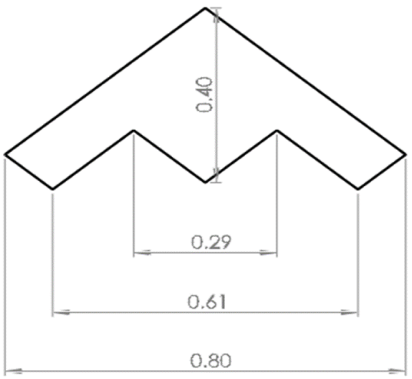

Figure 8: Planform and geometric parameters of Configuration 1

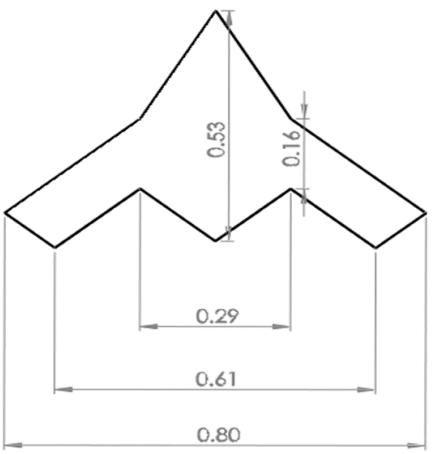

Figure 9: Planform and geometric parameters of Configuration 2

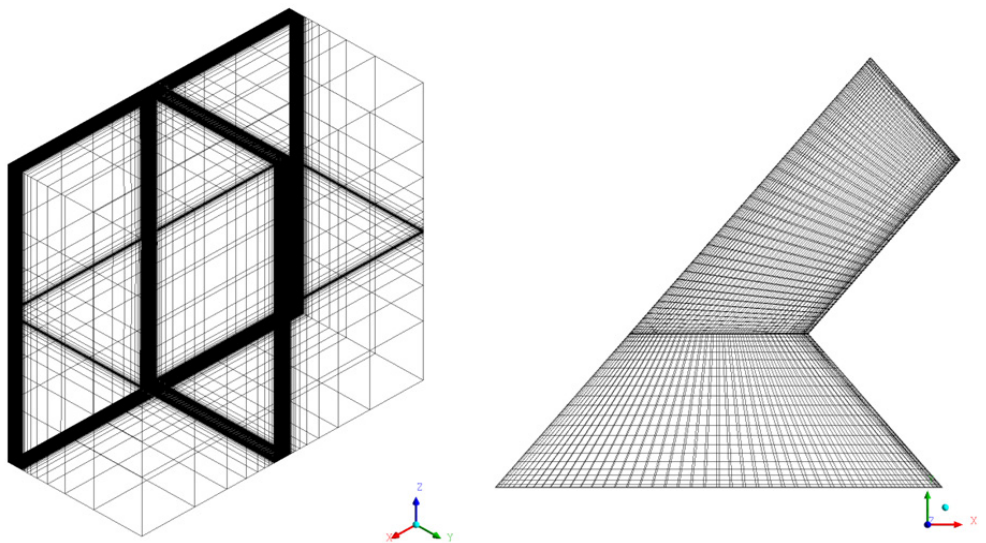

Figure 10: Computational grid for clean baseline Configuration 1

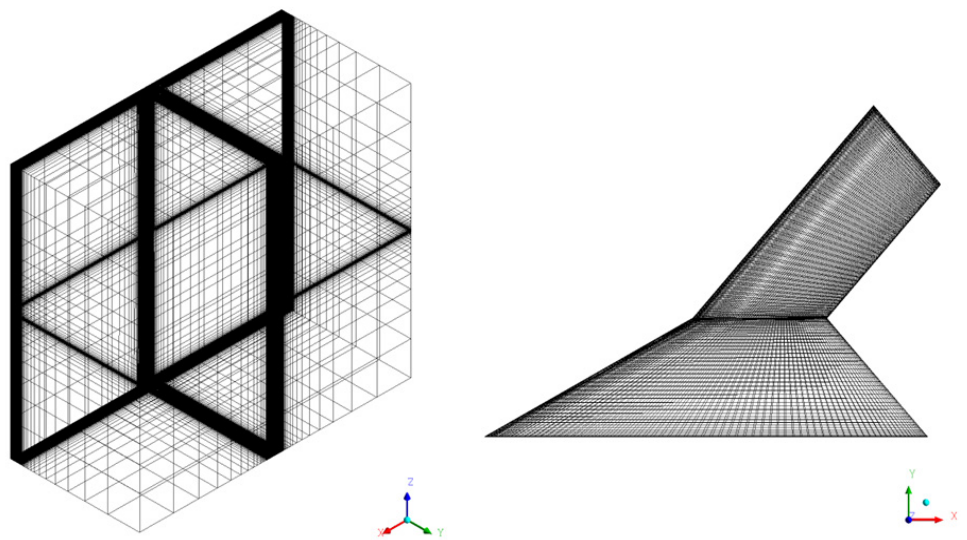

Figure 11: Computational grid for clean baseline Configuration 2

The near wall modelling significantly impacts the fidelity of numerical results. Solution variables have large gradients in the near-wall region, hence accurate representation of the flow in near-wall region determines the successful predictions of wall-bounded turbulent flows. In order to achieve good boundary layer resolution on surface of wall in the normal direction, first cell normal to wall was placed at 3.0e-6m for configuration 1, and for configuration 2 it was placed at 2.54e-6m. This resulted in Y+ values of less than 1 for both configurations, thus wall function approximations were not used in the solutions. For

configuration 1, little improvement in results was displayed with successive mesh refinements, therefore grid with half a million cells (0.5m) was chosen for the simulations of full flight envelop. For configuration 2, however, the flow has become more complicated due to the leading-edge strake. The successive mesh refinements have shown improvement in results but due to limited computational resources at hand, two million grid (2m) was chosen for the full flight envelop computations.

3.2.3. Solver settings

Fluent solver has the option to choose from either Pressure solver or Density based solver. For compressible and external flow simulations however, density based solver generally provide better accuracy. The two numerical solvers employ a similar discretisation process but pressure solver is different than density based solver in that it solves the governing equations sequentially; in other words the equations are segregated from one another. The density based solver solves all the equations simultaneously and as a result it consumes more memory. For this research, pressure solver was tested in the beginning but eventually density based solver was adopted for the computations in question.

Three dimensional problems in CFD take a long time to provide a converged solution. Therefore, in order to reduce simulation times, fluent solvers have implemented parallel processing capabilities. In this research, the parallel processing capabilities of the solvers were utilised for all the cases on local machines and as a result computation times were significantly reduced. Air is used as a fluid material with density following the ideal gas law. One equation Spalart-Allmaras turbulence model was used for all the computations under investigation. In Fluent the upwind scheme has the option to choose from either first order upwind scheme or second order upwind scheme. The first order upwind scheme makes it prone to numerical errors. Therefore, second order upwind scheme has been used for discretisation of computations in this study. Discretisation is a process in which partial differential equations are transformed into algebraic equations associated with discrete elements. The solution methods were based on implicit scheme in this report with Roe-FDS as flux type. A higher order accuracy is achieved in Fluent using finite volume formulation.

Standard initialisation was computed from far-field boundary condition. The solution of steady state RANS equations was achieved in an iterative manner. The convergence criteria for all the discretised equations was set to be 10-3. Please note, although all the simulations had achieved a minimum convergence criteria but in order to assess the convergence of solution, aerodynamic coefficients and moments were monitored as the solution progressed to its convergence criteria. Solution can only be considered converged when key parameters within problem show negligible change as solution progresses to its convergence criteria. In this study, coefficients of lift, drag and moments were monitored for all the computations in order to confirm the convergence of solution.

3.2.4. Vortex Lattice Method Approach

The Vortex Lattice Method (VLM) investigations in this study were performed using a software called Tornado. Tornado has a user interface that allows the user to interact directly with the programme. The functions within Tornado are displayed in the form of text menus. There are following four main menus in Tornado: Input operations, Lattice operations, computation operations and lastly Post processing and interactive operations. The first two

menus are part of the pre-processor of the code, second menu is the solver of the code and third menu is where post processing of the data is done. There is another menu called "Auxiliary operations" which contains help files and release information of the code. Tornado version 135 which was released in 2010 has been used for the investigations in this study.

In this study, geometry parameters and boundary conditions for configuration 1 and configuration 2 planforms were defined in pre-processor of the code by answering the sequence of questions. The mesh shown in Figure 12, was generated under lattice operations menu where there are two types of wake solvers: freestream following wake is a Tornado method and fixed wake is a standard VLM method. The main difference between the two methods is that Tornado has a freestream following wake which can be influenced by the angles of attack and sideslip. The wake coming off control surfaces and trailing edges of air vehicle is flexible and changes shape according to flight conditions, therefore Tornado method represented more realistic flow conditions and was chosen for this research. Computations were performed under "Computation operations" where sequential state parameter sweep menu was chosen; and solution for angles of attack ranging from α = -20˚ to 40˚ was obtained. In this module, solver applies Neumann boundary conditions and data is converted into forces and moments within each panel for the calculations of main results.

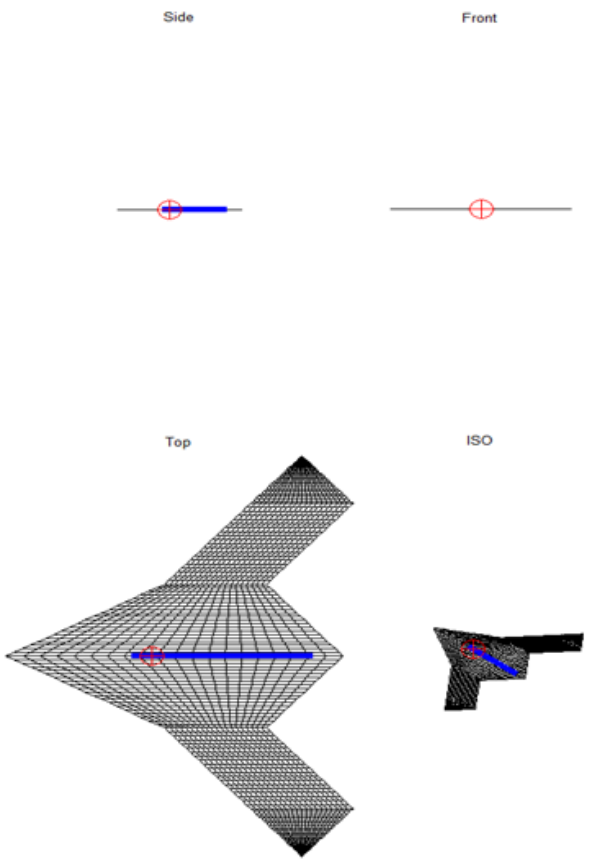

Figure 12: VLM mesh generated in Tornado (Configuration 2)

4. RESULTS AND DISCUSSION

4.1. Baseline Configurations

Linear computational results were investigated with the VLM Tornado code, and non-linear computational studies were performed with in-house and commercial CFD codes. These numerical results will be discussed and compared with experimental data in this section. For all viscous computations, fully turbulent flow was assumed and the Spalart-Allmaras turbulence model was used to close the governing equations. The freestream conditions are provided by the wind tunnel tests where Mach number was 0.1 and the Reynolds number based on aerodynamic mean chord length was 5×105. Aerodynamic coefficients and moments were measured as a function of the angle of attack ranging from $-20^{\circ} \leq \alpha \leq 40^{\circ}$. From Figure 13, the aerodynamic characteristics of flying-wing configurations are shown to be a strong function of the sweep angle; by increasing the leading-edge sweep angle of configuration 2 to 60°, an increase in lift was noticed at higher angles of attack. The stall was also delayed to higher incidence angle of 29° by increasing the sweep angle of configuration 2. Therefore configuration 2 was considered a better planform model for the flow control problem. Figure 14 shows Y^{+} distribution on the suction side of both configurations at an angle of attack of 30°. It can be seen that Y^{+} values for both configurations are below 1. This results in adequate resolution of boundary layer for the configurations under investigation. The predicted computational lift, drag and moment coefficients are shown in figures 15, 16 and 17 and results are compared with experimental data. The figures show the angles of attack range from $\alpha = -10^{\circ}$ to 40°. Lift coefficient plots show a linear behaviour up to the angles where wings stall occur.

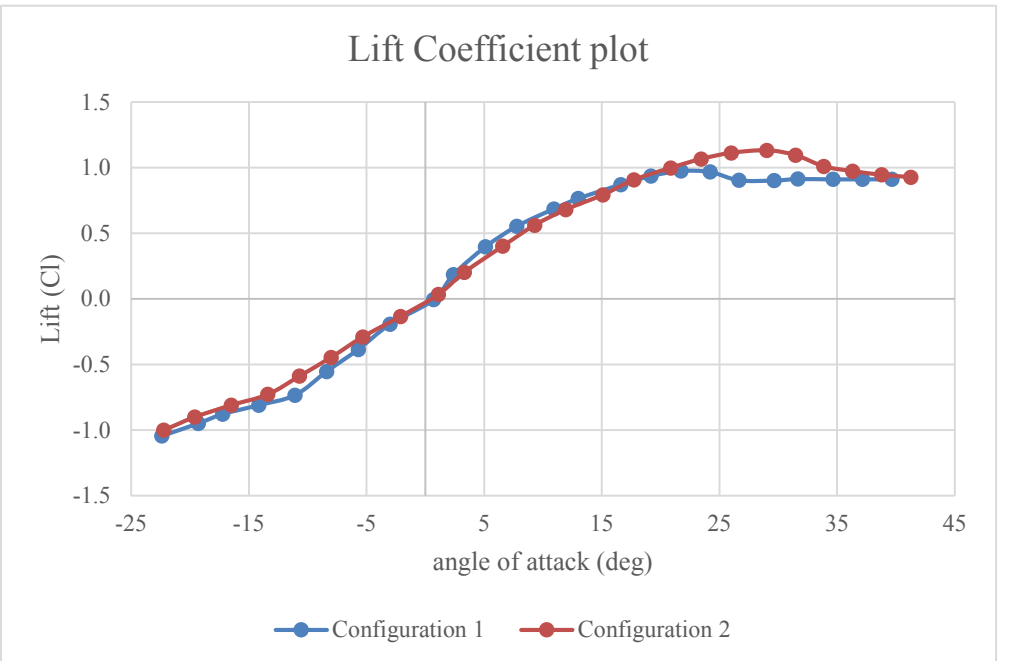

Figure 13: Experimental coefficient of lift comparison between Configuration 1 and Configuration 2 flat plate models

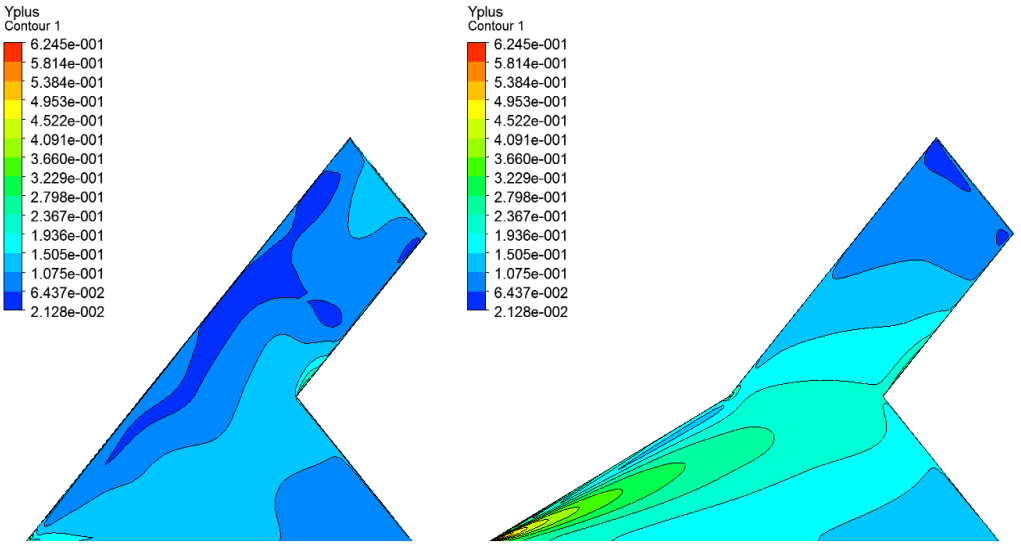

Figure 14: Y+ distribution on suction sides of Configuration 1 (left) and Configuration 2 (right) at an angle of attack of 30°

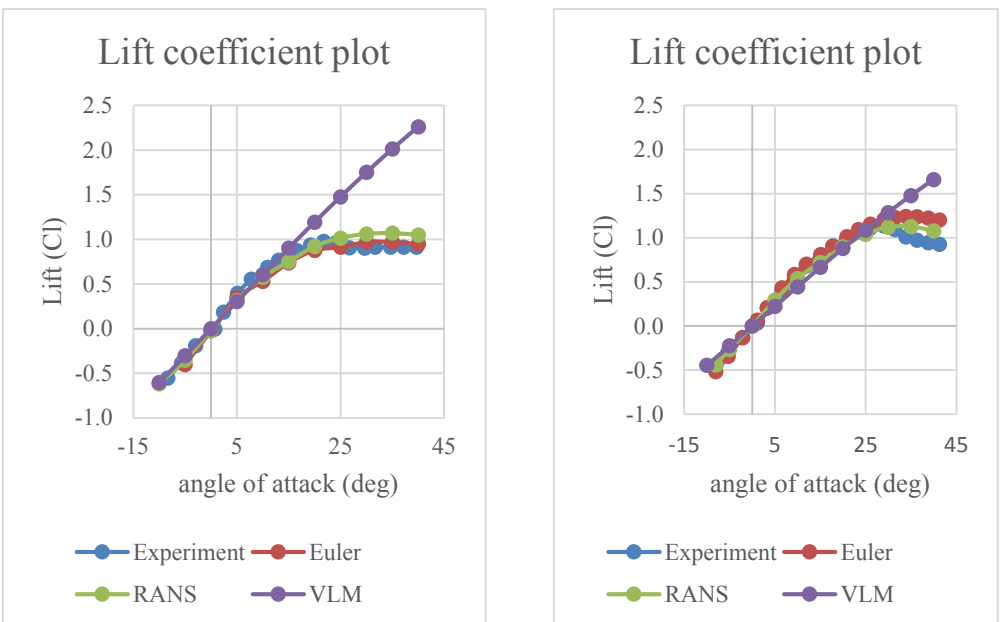

Figure 15: Lift coefficient vs angle of attack are shown: 40° configuration 1 (left) and 40° with 60° strake configuration 2 (right)

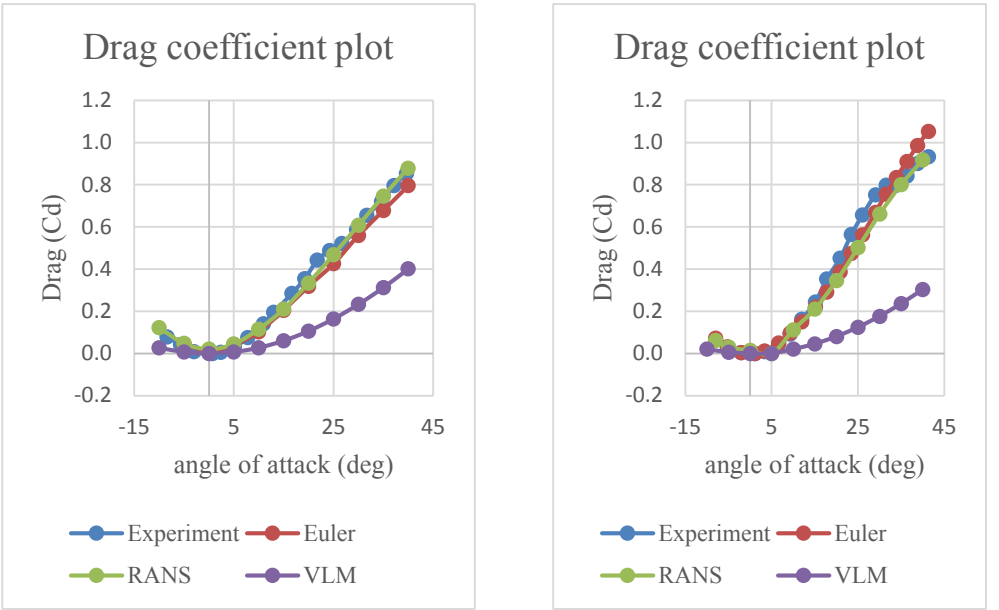

Figure 16: Induced-drag coefficient vs angle of attack are shown: 40° configuration (left) and 40° with 60° strake configuration (right)

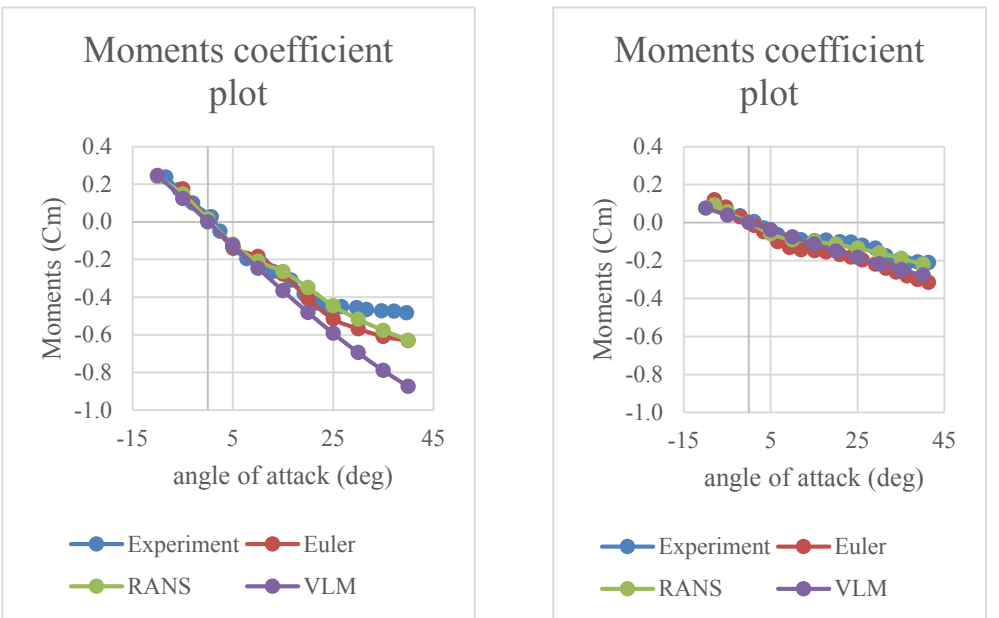

Figure 17: Pitching-moment coefficient vs angle of attack are shown: 40° configuration (left) and 40° with 60° strake configuration (right)

The drop in lift starts appearing after the stall angles, but unlike the deep stall at high Reynolds number as is the case with rectangular and other planform wings, the stall is not abrupt which is the main characteristics of flying-wing configurations. Lift drop for configuration 1 was even less abrupt than configuration 2. The pitching moments were calculated at quarter chord point from the leading edge of the wing. It can be seen from moment plots that moment coefficient decreases as angle of attack is increased. The VLM predicts only linear variation of lift and pitching moments with incidence angle, and substantially under-predicts the induced drag. The drag is predicted quite well by non-linear computations Euler and RANS methods. The VLM methods assume the flow to be fully attached to the surface, which is not the case for configurations under investigation. Computation using the Euler equations are better able to capture the separated-vortex flow behaviour and the maximum-lift characteristics. Results obtained from a RANS method generally give a similar level of agreement with experiment to the Euler results.

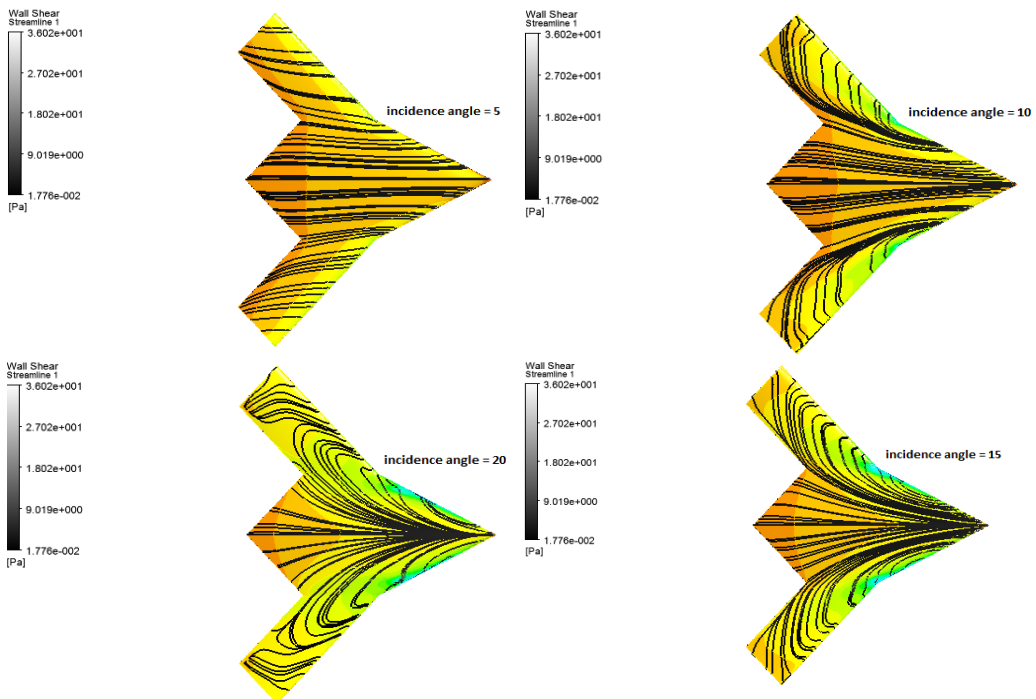

Figure 18: Pressure distribution and surface streamlines on upper surface of Configuration 2

The flow field on configuration 2 was visualised using surface streamlines as shown in Figure 18. In CFD, an illustration of streamlines is an excellent tool for examining the nature of a flow field. A streamline is defined as a curve whose tangent is in the direction of velocity vector at that point [12]. In order to present more realistic flow field conditions, the model with aerofoil profiles will be presented in this section. The highly swept wings of flying-wing configurations promote separated-vortex flows on such air vehicles. Leading edge vortices enhance the lift and delay the stall to a higher angle, but this additional lift cannot be exploited due to forward migration of flow to the outboard sections of the wing. In figure 18 static

pressure distribution and friction streamlines have been presented on upper surface of Configuration 2 for angles of attack ranging from $\alpha = 5^{\circ}$ to 20°. It can be observed that as angle of attack is increased the migration to outer panels become more severe. This results in loss of lateral control because control surfaces are essentially operating in separated flow. One of the objectives of this research is to control the forward migration of flow to the outboard sections of flying-wing which will result in effective lateral control at higher angles of attack [11].

4.2. Flow control results

The leading edge flap or slat has been used in past to increase the maximum lift coefficient and delay the stall angle to a higher angle of attack [12] [8]. In present study, however, the leading edge slot was used for the purpose of passive flow control on a flying-wing configuration. Although leading edge flap or slat could also be used to create an airflow barrier for boundary layer separation, but it should be avoided on a flying-wing configuration due to its adverse effect on RCS signature of an air vehicle [10]. An alternative to separate slat was to cut a slot near the leading edge of the wing to form a slotted wing as shown in Figure 19(a). The slots are easier to construct in a flying-wing configuration and are less likely to give operational troubles than movable flaps. The reason behind the construction of slots was to route high pressure air through the gap in order to create an airflow barrier for the spanwise flow on the suction side of the wing. Therefore, in addition to primary flow over the suction side, there is now a secondary flow which takes place through the gap of the slot. This secondary flow follows the contours of the surface of the wing and channel more airflow to the control surfaces, which in turn enhance the lateral control of the vehicle [12] [8] [9]. In order to achieve this objective, leading edge slots were created in configuration 2 and an experimental investigation was conducted in a low speed wind tunnel, where aerodynamic forces and moments were measured as a function of angle of attack and results were compared with clean baseline model. This served two-fold purpose of elucidating relevant high-lift characteristics of a slotted wing and provided experimental data for validation and evaluation of computational methods. The width of leading-edge slot was 0.002m and length was 0.2m, and it was chamfered on the edges in order to aid the airflow to flow from lower to upper surface of the wing.

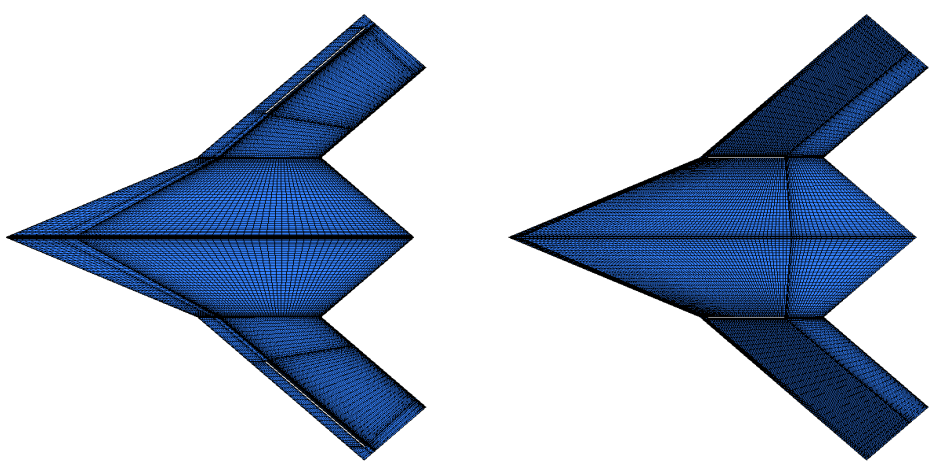

Figure 19: Configuration 2 with Leading-Edge Slot (a); Cross Flow Slot (b)

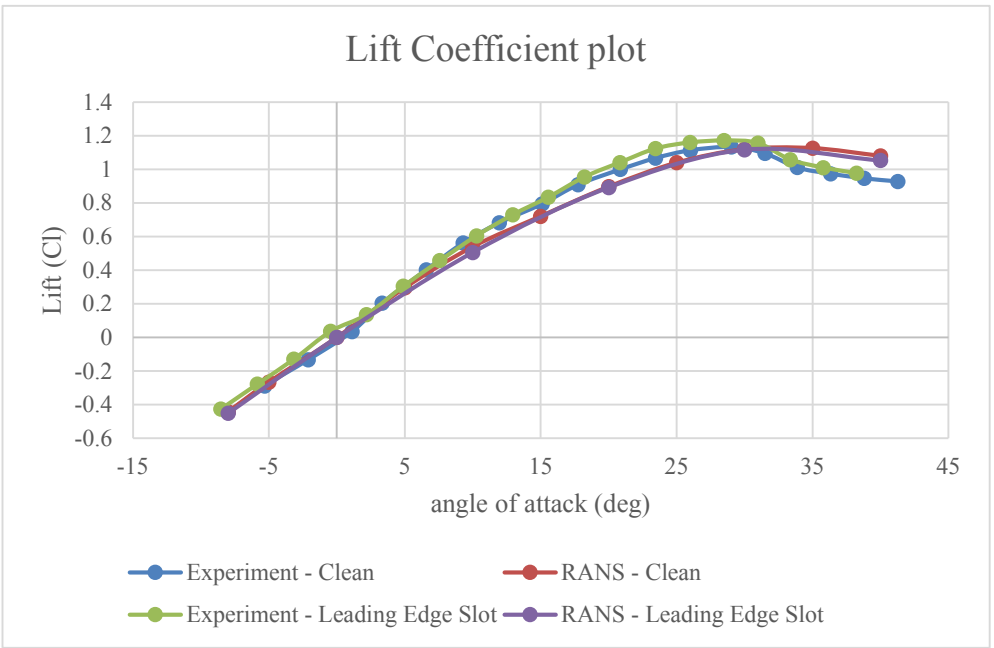

Figure 20: Comparison of lift coefficient plot between clean and leading-edge slot models

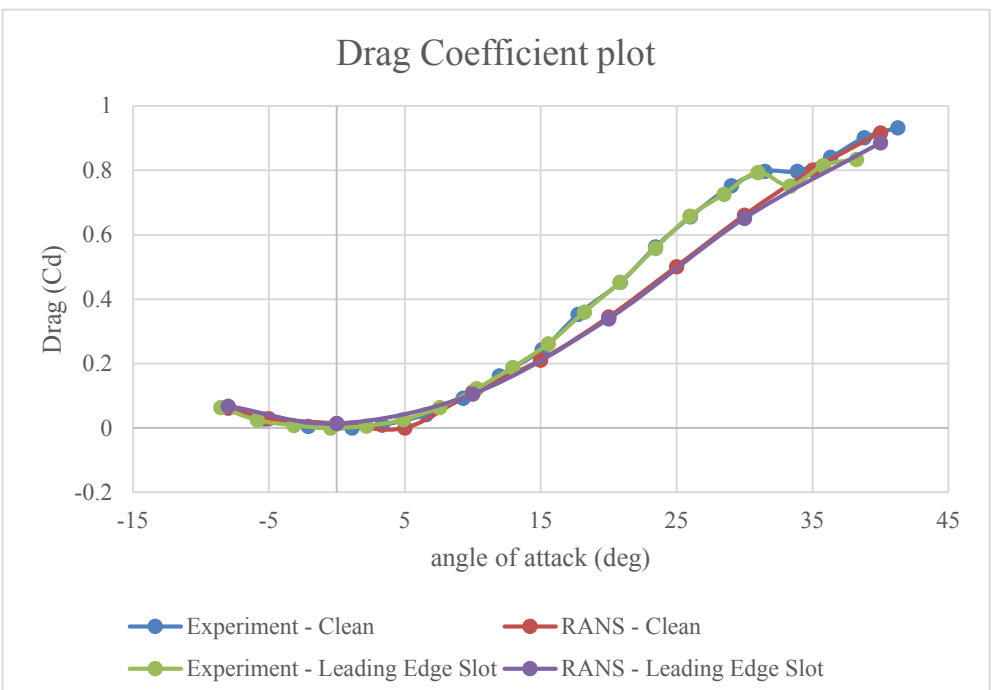

Figure 21: Comparison of drag coefficient plot between clean and leading-edge slot models

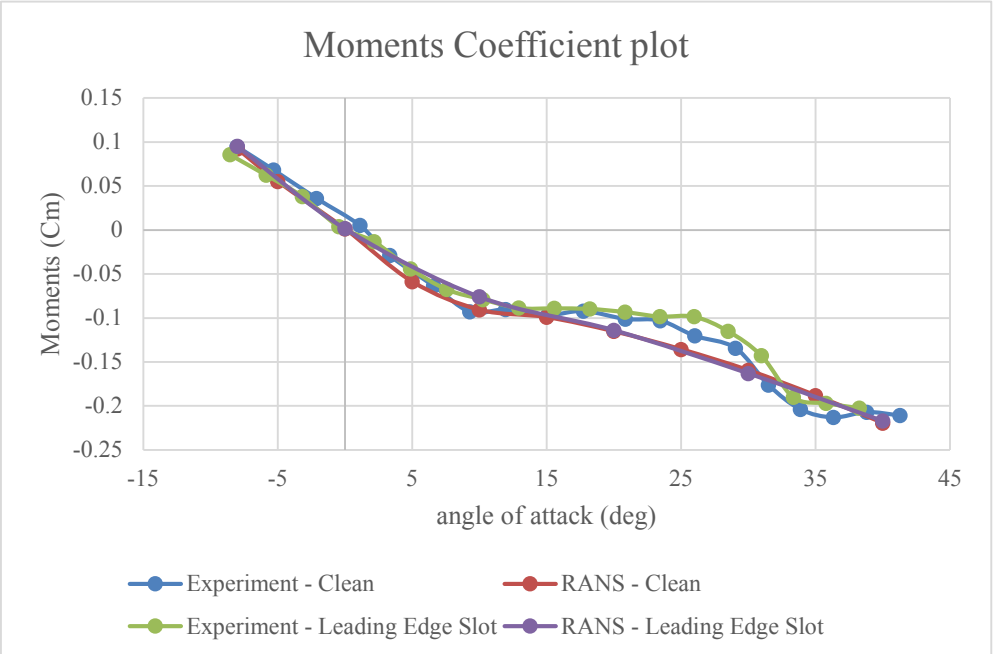

Figure 22: Comparison of drag coefficient plot between clean and leading-edge slot models

The CFD simulations of a slotted wing were performed and results were compared with experimental data as shown in Figures 20, 21 and 22. The figures show the angles of attack range from $\alpha = -8^{\circ}$ to 40°. The purpose of these experimental and computational investigations was to determine the effect of leading-edge slots on the aerodynamic characteristics of configuration 2. The CFD results are in good agreement with the data obtained from a low speed wind tunnel tests. The investigations have predicted a slightly higher maximum lift coefficient for the model with a leading-edge slot but induced drag and pitching moments have produced similar results to the clean baseline model. If slots are permanently open, the extra drag at high speeds is a disadvantage. Therefore, for high speed cruise conditions, the slots can be fitted with a closing valve or a device operated by a control mechanism [21]. From the results of tests with a leading-edge slot, it seems very probable that the maximum lift coefficient of the device can be still furthered improved by varying the width, gap and position of the slot in relation to leading edge of the wing . As is the case with conventional leading edge flap, a proper leading-edge slot must be created so that it ejects a flow nearly parallel to the suction side and sits at the right position in relation to leading edge of the wing [8]. The purpose of this research, however, is not to increase maximum lift coefficient but to create an airflow barrier in order to reduce the intensity of forward migration of leading edge vortices to the outer panels of the vehicle. If more airflow is channelled to the control surfaces located near trailing edges, the lateral control of the vehicle can be enhanced at high angles of attack regime.

The flow field on the suction side of a slotted flying-wing configuration was visualised using surface streamlines and results were compared with clean baseline model. A streamline is the path followed by a particle of an oil drop when air blows it in a steady airflow, but one

streamline cannot cross another [12]. In Figure 23, surface streamline comparison between a clean baseline model and a leading-edge slot model at an incidence angle of 5˚ is shown. When streamlines are shown together it indicates increased velocity, and when streamlines are wide apart it represents decreased velocity. When streamlines converge, it means the fluid has accelerated and it has detached from the surface of the wing. On the contrary when they diverge, it indicates decelerating airflow and the associated rise in the pressure [22]. It can be seen from the streamline pattern that fluid has converged near the upper part of leading-edge slot, thus re-energising the boundary layer and channelling more fluid towards the control surfaces located near trailing edges the of vehicle. The leading-edge slot method was found to be ineffective at higher angles of attack when intensity of forward migration of leading edge vortices became more severe.

In order to control flow at higher angles of attack, another novel technique of cross-flow slot was implemented on the representative flying-wing configuration. The slot has a width of 0.002m and a length of 0.1m, and it has chamfered edges. The current research has focused on using thin plates which project up from the wing to prevent the spanwise flow on a flying-wing configuration. An example of this has been shown in a delta wing air-vehicle in Figure 2 of this paper. The vertical surfaces, however, must be avoided as they create a detrimental effect on RCS signature of an air vehicle. The advantage of cross-flow slot is that it is flushed with the surface of the wing, therefore it is going to have a much smaller RCS signature than a vertical surface. The picture of a meshed cross-flow slot model is shown in Figure 19(b). In Figure 24, surface streamline comparison between a clean baseline model and a cross-flow slot model at an angle of attack of 25˚ is shown. The streamline pattern in Figure 24 has depicted a generation of a vortex next to cross-flow slot, which has energised the flow field and as a result more air flows over the control surfaces of the vehicle. It can also be seen that very little fluid has migrated forward towards the outer panels, and most of the air was channelled towards the tips of the wing. This will make the spoilers of air vehicle more effective at higher angles of attack. Therefore, it was decided that further research on cross-flow slot will be carried out, and the optimum location and size of the slot will be investigated using a CFD optimiser.

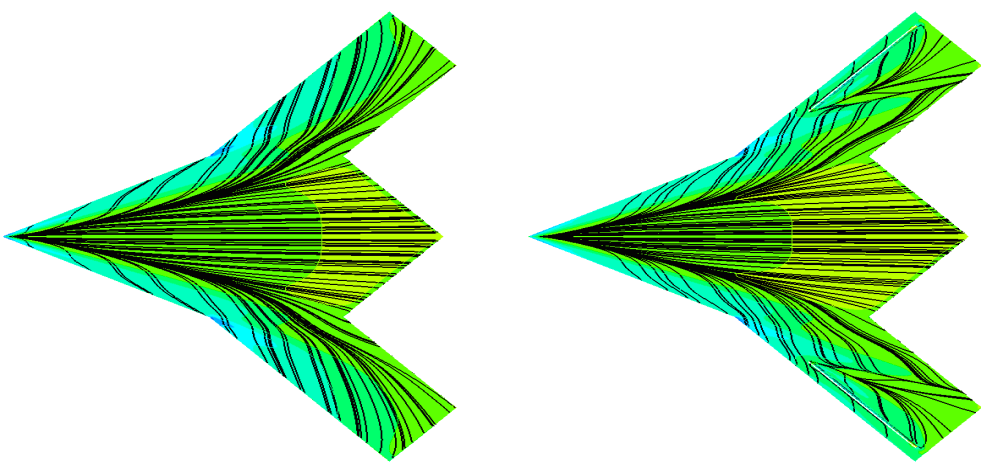

Figure 23: Surface streamlines comparison between a baseline model and a leading edge slot model at incidence angle of 5 degrees

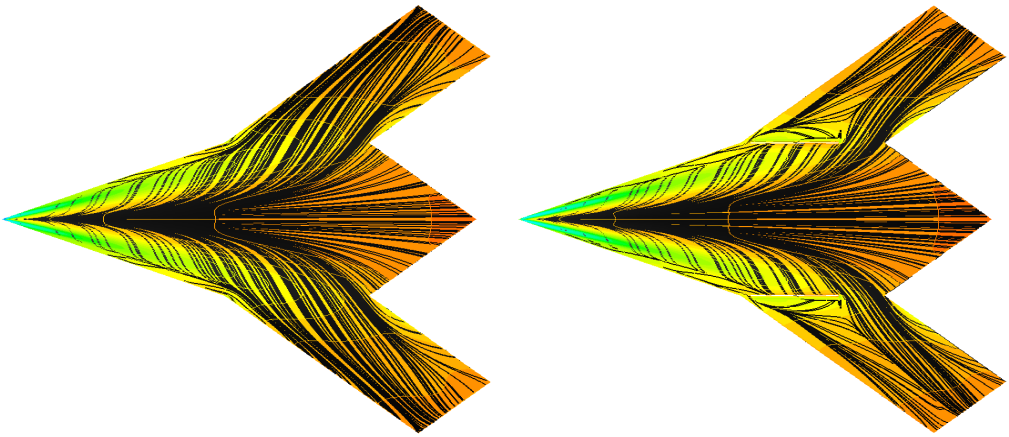

Figure 24: Surface streamlines comparison between baseline and cross flow cavity models at incidence angle of 25 degrees

5. CONCLUSION

Standard techniques for passive flow-control [6] [7] [8] [9] have a detrimental effect on RCS, therefore cannot be used in this study. Instead leading-edge and cross-flow slots are considered because they have a reduced RCS signature.

Experimental and computational investigations on leading-edge slots were performed, and it was found that the leading-edge slot technique worked for low angles of attack but was ineffective for flying-wing configurations at high angles of attack.

At higher angles of attack, another novel flow-control techniques called cross-flow slot method was implemented on a generic flying-wing configuration. The CFD investigations on representative configuration has shown better lateral flow-control results for this technique.

For future work, the optimum location and size of the cross-flow slot will be investigated using a CFD optimiser and the optimised results will be validated with a low speed wind tunnel.

REFERENCES

[1] Schütte, A., D. Hummel, and S.M. Hitzel, Flow Physics Analyses of a Generic Unmanned Combat Aerial Vehicle Configuration. Journal of Aircraft, 2012. 49(6): p. 1638-1651.

[2] Bertin, J.J., Aerodynamics for Engineers. 4th ed. 2002, USA: Prentice Hall.

[3] Gudmundsson, S., Chapter 9 - The Anatomy of the Wing, in General Aviation Aircraft Design, S. Gudmundsson, Editor. 2014, Butterworth-Heinemann: Boston. p. 299-399.

[4] Frink, N.T., M. Tormalm, and S. Schmidt, Three Unstructured Computational Fluid Dynamics Studies on Generic Unmanned Combat Aerial Vehicle. Journal of Aircraft, 2012. 49(6): p. 1619-1637.

[5] Shevell, R.S., Fundamentals of Flight. 2nd ed. 1989, New Jersey: Prentice Hall.

[6] Buchholz, M.D. and J. Tso, Lift Augmentation on Delta Wing with Leading-Edge Fences and Gurney Flap. Journal of Aircraft, 2000. 37(6): p. 1050-1057.

[7] Anderson, D.F., Understanding flight. 2nd ed. ed, ed. S. Eberhardt. 2010, New York: New York : McGraw-Hill.

[8] Kermode, A.C., Mechanics of flight. 12th ed / rev. by R.H. Barnard and D.R. Philpott. ed, ed. R.H. Barnard and D.R. Philpott. 2012, New York: Pearson Education.

[9] Gudmundsson, S., Chapter 10 - The Anatomy of Lift Enhancement, in General Aviation Aircraft Design, S. Gudmundsson, Editor. 2014, Butterworth-Heinemann: Boston. p. 401-457.

[10] Coppin, J., Aerodynamics, Stability and Shape Optimisation of Unmanned Combat Air Vehicles, in Department of Mechanical Engineering. 2014, University of Sheffield.

[11] Robert, N., et al., Modification of the Flow Structure over a UAV Wing for Roll Control, in 45th AIAA Aerospace Sciences Meeting and Exhibit. 2007, American Institute of Aeronautics and Astronautics.

[12] Anderson, J.D., Fundamentals of Aerodynamics. 2010, Boston: McGraw-Hill Education.

[13] Wilson, H.A. and J.C. Lovell, Full-scale Investigation of the Maximum Lift and Flow Characteristics of an Airplane Having Approximately Triangular Plan Form. 1947.

[14] Earnshaw, P.B., An experimental investigation of the structure of a leading-edge vortex, M.o. Aviation, Editor. 1961.

[15] Polhamus, E.C., Predictions of vortex-lift characteristics based on a leading-edge suction analogy, in 6th Annual Meeting and Technical Display. 1969, American Institute of Aeronautics and Astronautics.

[16] Elkhoury, M. and D. Rockwell, Visualized Vortices on Unmanned Combat Air Vehicle Planform: Effect of Reynolds Number. Journal of Aircraft, 2004. 41(5): p. 1244-1247.

[17] Kingsley, S. and S. Quegan, Understanding Radar Systems. 1992, Berkshire: Mcgraw-Hill.

[18] Jenn, D.C., Radar and laser cross section engineering. 1995, Washington, DC: American Institute of Aeronautics and Astronautics.

[19] Johnston, L.J., High-Lift Aerodynamics of Uninhabited Combat Air Vehicle Configurations with Reduced Radar Cross-Section Characteristics, in RAES Applied Aerodynamics Conference. July 2012: Bristol.

[20] Gad-el-Hak, M., Flow Control: Passive, Active, and Reactive Flow Management. 2000, New York: Cambridge University Press.

[21] Lachmann, G., Results of Experiments with Slotted Wings. 1924, NACA.

[22] Johnson, R.W., The handbook of fluid dynamics. 1998, Heidelberg: Springer-Verlag.